On the isospin 0 and 1 resonances from $\pi\Sigma$ photoproduction data

L. Roca[1] and E. Oset[2]
[1] *Departamento de Física, Universidad de Murcia, E-30100 Murcia, Spain.* [2] *Departamento de Física Teórica and IFIC, Centro Mixto Universidad de Valencia-CSIC, Institutos de Investigación de Paterna, Aptdo. 22085, 46071 Valencia, Spain*

(Dated: July 29, 2013)

Recently we presented a successful strategy to extract the position of the two $\Lambda(1405)$ poles from experimental photoproduction data on the $\gamma p \to K^+\pi^0\Sigma^0$ reaction at Jefferson Lab. Following a similar strategy, we extend the previous method to incorporate also the isospin 1 component which allows us to consider in addition the experimental data on $\gamma p \to K^+\pi^\pm\Sigma^\mp$. The idea is based on considering a production mechanism as model independent as possible and implementing the final state interaction of the final meson-baryon pair based on small modifications of the unitary chiral perturbation theory amplitudes. Good fits to the data are obtained with this procedure, by means of which we can also predict the cross sections for the $K^-p \to \bar{K}N$, $\pi\Sigma$, $\pi\Lambda$ reactions for the different charge channels. Besides the two poles found for the $\Lambda(1405)$ resonance, we discuss the possible existence of an isospin 1 resonance in the vicinity of the $\bar{K}N$ threshold.

I. INTRODUCTION

In a recent paper [1] we analyzed the CLAS data for photoproduction of the $\Lambda(1045)$ [2] in the reaction $\gamma p \to K^+\pi^0\Sigma^0$, which filters I=0 for the $\pi^0\Sigma^0$ state, where clear peaks where seen related to the $\Lambda(1045)$ excitation. The aim was to determine the mass and width of the two $\Lambda(1405)$ states, predicted by all the latest works based on chiral dynamics. While the nature of the $\Lambda(1045)$ as generated from the interaction of meson baryon channels with strangeness S=-1 has been long accepted [3–5], the use of chiral dynamics and unitary schemes brought new light into this issue [6–22], and the $\Lambda(1045)$ appears in all these works by using chiral Lagrangians and adjusting a minimum amount of parameters to reproduce $\bar{K}N$ data. Hints of the existence of two, rather than one states were found in [9, 23] and a thorough study of the existence of two poles was conducted in [13]. Since then, all the new works on chiral dynamics obtain two poles and this has come as a broadly accepted fact, even reflected in the PDG [24].

All works on chiral dynamics fit $\bar{K}N$ data to determine the few free parameters of the theory and then determine the position of the poles. Some also consider data on $\Lambda(1405)$ production, like [17]. The omission of $\Lambda(1405)$ production data in most works was justified because of the nontrivial dynamics of the reaction process, although work in this direction has been done [7, 25–29]. However, the novelty of [1] was to show that the $\Lambda(1405)$ photoproduction data by themselves had the capacity to provide the pole positions of the two $\Lambda(1405)$ states which were found around 1385-68i MeV and 1419-22i MeV. The analysis of these data also allowed to predict the cross section for the $K^-p \to \pi^0\Sigma^0$ reaction in good agreement with data, without using the data of that reaction in the fit. While in all known reactions the two poles do not revert into two peaks, but only in different shapes [2, 30–39], the new data on electroproduction [40], with two visible peaks around 1368 MeV and 1423 MeV, have been an unexpected surprise. The lower pole is also broader than the higher one, as extracted from the photoproduction data in [1].

In the present paper we shall follow the strategy of [1] and use only the photoproduction data of the $\gamma p \to K^+\pi^\pm\Sigma^\mp$ reactions measured in [2] in order to extract the isospin I=1 amplitude in addition to the I=0 one extracted in [1] from the $\gamma p \to K^+\pi^0\Sigma^0$ data alone. This will allow us to shed light on the possible I=1 state around the $\bar{K}N$ threshold which has been often advocate. Indeed, in [9] hints of the existence of such state were discussed. The state became fuzzy in the analysis of [13], showing up with sets of parameters with small SU(3) breaking, and reverting into a cusp with full SU(3) breaking. Some experimental support for such state has also been provided in [41, 42]. On the other hand, once again we will show that the data on photoproduction contain by themselves enough information to provide both the I=0 and I=1 amplitudes, by means of which, and without fitting the data, good results are obtained for the $\bar{K}N$ scattering amplitudes. The analysis conducted here will shows that, while no clear pole is found in the second Riemann sheet for the I=1 state (while a pole is found in another unphysical Riemann sheet), the amplitude in this channel is strong enough and has obvious repercussion in the photoproduction data, producing a clear split of the $\gamma p \to K^+\pi^\pm\Sigma^\mp$ cross sections. Whether there is pole or not, the I=1 amplitude shows a clear enhancement close to the $\bar{K}N$ threshold and is visible as a pronounced cusp as a consequence of a strong attraction, in the border line of creating a quasibound bound $\bar{K}N$ state. We show that the situation is very similar to the one of the $a_0(980)$ resonance, which is accepted as a resonance. The fact remains that whether one decides to call it or not a resonance, the resonant like structure in the real axis has important repercussion in the photoproduction amplitudes and similarly can have relevant effects in many other observables.

II. UNITARIZED MESON-BARYON AMPLITUDE

The main ingredient of our analysis are the meson baryon amplitudes from the chiral unitary approach. There are many references where the details for the construction of the meson-baryon unitarized amplitude can be found, (see for instance refs. [8, 9, 11, 43]). It was also summarized in ref. [1] for the $I = 0$ case. We next review it for the sake of completeness and including in addition the evaluation of the $I = 1$ channel.

The lowest order chiral Lagrangian for the interaction of the octet of Goldstone bosons with the octet of the low lying $1/2^+$ baryons [44] provides the following tree level transition amplitudes in s-wave [11]:

$$V_{ij}^I(\sqrt{s}) = -C_{ij}^I \frac{1}{4f^2}(2\sqrt{s} - M_i - M_j) \times \left(\frac{M_i + E_i}{2M_i}\right)^{1/2} \left(\frac{M_j + E_j}{2M_j}\right)^{1/2}, \quad (1)$$

where the superscript I stands for the isospin, $\sqrt{s}$ the center of mass energy, f the averaged meson decay constant $f = 1.123 f_\pi$ [11] with $f_\pi = 92.4$ MeV, E_i (M_i) the energies (masses) of the baryons of the i-th channel. The C_{ij}^0 coefficients, for isospin $I = 0$, are given by

$$C_{ij}^0 = \begin{pmatrix} 3 & -\sqrt{\frac{3}{2}} \\ -\sqrt{\frac{3}{2}} & 4 \end{pmatrix}. \quad (2)$$

The i and j subscripts represent the channels $\bar{K}N$ and $\pi\Sigma$ in isospin-basis. Note that we do not consider the other possible channels in $I = 0$, $\eta\Lambda$ and $K\Xi$, for the sake of simplicity of the approach and because for the energies that we will consider in this work the effect of those channels can be effectively reabsorbed in the subtraction constants. The coefficients for isospin $I = 1$ are

$$C_{ij}^1 = \begin{pmatrix} 3 & -1 & -\sqrt{\frac{3}{2}} \\ -1 & 2 & 0 \\ -\sqrt{\frac{3}{2}} & 0 & 0 \end{pmatrix}. \quad (3)$$

where the order of the channels are $\bar{K}N$, $\pi\Sigma$ and $\pi\Lambda$. We also neglect here the $\eta\Sigma$ and $K\Xi$ states into the coupled channels equations since their thresholds are also very far from the energy region of interest in the present work.

The chiral unitary approach is based on the implementation of unitarity of the scattering amplitude in coupled channels and the exploitation of its analytic properties. This is usually accomplished by means of the Inverse Amplitude Method [45, 46] or the N/D method [9, 47, 48]. In this latter work the equivalence with the Bethe-Salpeter equation used in [49] was established. Based on the N/D method, the coupled-channel scattering amplitude T_{ij} is given by the matrix equation

$$T = [1 - VG]^{-1} V, \quad (4)$$

where V_{ij} is the interaction kernel of Eq. (1) and the function G_i, or unitary bubble, is given by the dispersion integral of the two-body phase space $\rho_i(s) = 2M_i q_i/(8\pi W)$, in a diagonal matrix form, with M_i the mass of the baryon of the meson baryon loop, q_i the on shell momentum of the particles of the loop and W the center of mass energy.

This G_i function is equivalent to the meson-baryon loop function

$$G_i = i \int \frac{d^4q}{(2\pi)^4} \frac{M_i}{E_i(\vec{q})} \times \frac{1}{k^0 + p^0 - q^0 - E_i(\vec{q}) + i\epsilon} \frac{1}{q^2 - m_i^2 + i\epsilon}. \quad (5)$$

This integral is logarithmically divergent, and therefore it must be regularized, which is usually carried out either with a three momentum cutoff or with dimensional regularization in terms of a subtraction constant a_i. The connection and equivalence between both methods was shown in Refs. [9, 46]. In ref. [11, 13] the values $a_{KN} = -1.84$, $a_{\pi\Sigma} = -2$ where used for the $I = 0$ channels. In the present case, since we do not consider the $\eta\Lambda$ and $K\Xi$ channels, these subtraction constants may differ slightly but we will allow to vary these constants in the fit below. For the $I = 1$ channels, in ref.[50] the same value for a_{KN}, $a_{\pi\Sigma}$ as in the $I = 0$ case was used and $a_{\pi\Lambda} = -1.83$ for the new channel in the $I = 1$.

The amplitudes $T_{\bar{K}N\to\pi\Sigma}$ and $T_{\pi\Sigma\to\pi\Sigma}$ for $I = 0$ are depicted in fig. 1. They produce two poles in the second Riemann sheet of the complex energy plane at the positions $\sqrt{s_0} = 1387 - 67i$ MeV, and $1437 - 13i$ MeV. Note that the poles come dynamically from the non-linear dynamics involved in the implementation of unitarity in the meson-baryon scattering amplitude, without the need to include the poles as explicit degrees of freedom. This is what is usually called *dynamically generated* resonance or meson-baryon molecule. It is worth mentioning that the

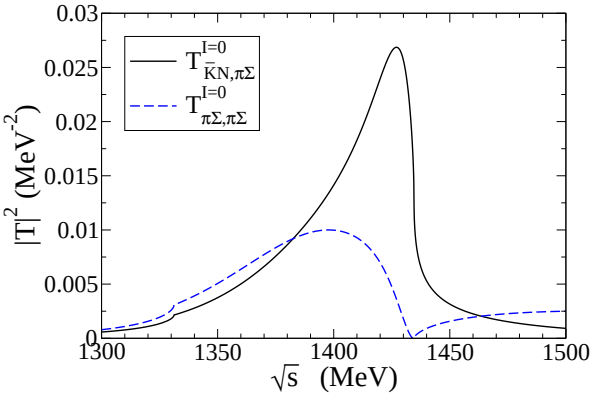

FIG. 1. (Color online) Modulus squared of the $I = 0$ meson-baryon unitarized amplitudes $T^{I=0}_{\bar{K}N,\pi\Sigma}$ (solid line) and $T^{I=0}_{\pi\Sigma,\pi\Sigma}$ (dashed line).

unitarized amplitudes provide the actual meson-baryon

scattering amplitudes, not only the poles of the resonance in the complex plane. Indeed the resonant shapes of the amplitudes around the 1400 MeV region are far from looking like Breit-Wigner shapes. Therefore fits to experimental data assuming Breit-Wigner resonant shapes are not suitable for this resonance and a model like the present one, in the line of implementing unitarity in coupled channels, is called for in order to reproduce or fit experimental data where these amplitudes are relevant. In fig. 2 we show the amplitudes $T_{\bar{K}N\to\pi\Sigma}$, $T_{\pi\Sigma\to\pi\Sigma}$ and

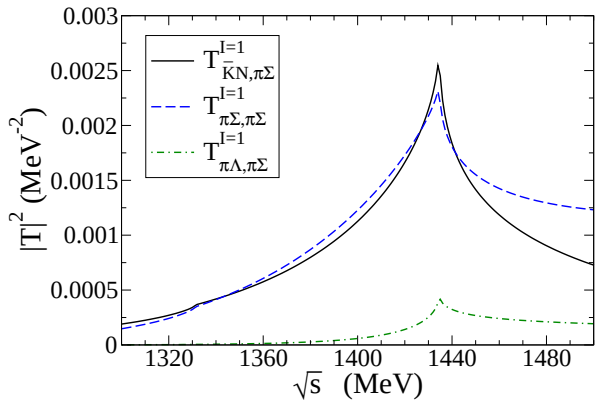

FIG. 2. (Color online) Modulus squared of the $I = 1$ meson-baryon unitarized amplitudes $T^{I=1}_{\pi\Sigma,\pi\Sigma}$ (solid line), $T^{I=1}_{\bar{K}N,\pi\Sigma}$ (dashed line) and $T^{I=1}_{\pi\Lambda,\pi\Sigma}$ (dashed-dotted line) .

$T_{\pi\Sigma\to\pi\Lambda}$ in $I = 1$. In this case there is no pole associated to the visible increase of strength appreciable at threshold in the amplitudes. We will elaborate further on this issue later on and we will discuss on the possible connexion to an actual $I = 1$ resonance in the next section.

III. FIT TO PHOTOPRODUCTION DATA

In our previous work [1] we only considered the $\gamma p \to K^+\pi^0\Sigma^0$ data of [2] since this particular reaction filters the $I = 0$ and therefore these were the only data used in [1]. However, in the present work we are also interested in the $I = 1$ channel in order to try to make conclusions from a possible resonance in $I = 1$. If one looks at the isospin decomposition of the final $\pi\Sigma$ states,

$$
\begin{aligned}
|\pi^0\Sigma^0\rangle &= \sqrt{\frac{2}{3}}|2\,0\rangle - \frac{1}{\sqrt{3}}|0\,0\rangle,\\
|\pi^+\Sigma^-\rangle &= -\frac{1}{\sqrt{6}}|2\,0\rangle - \frac{1}{\sqrt{2}}|1\,0\rangle - \frac{1}{\sqrt{3}}|0\,0\rangle,\\
|\pi^-\Sigma^+\rangle &= -\frac{1}{\sqrt{6}}|2\,0\rangle + \frac{1}{\sqrt{2}}|1\,0\rangle - \frac{1}{\sqrt{3}}|0\,0\rangle,
\end{aligned}
\tag{6}
$$

it is clear then that one must also include the $\gamma p \to K^+\pi^+\Sigma^-$, $\gamma p \to K^+\pi^-\Sigma^+$ in the analysis.[1]

The main observable measured for this reaction is the $\pi\Sigma$ invariant mass distribution for the different allowed charge combinations (see fig. 4 below).

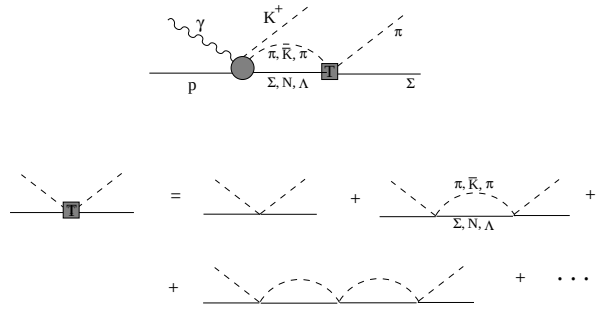

FIG. 3. General mechanisms for the photoproduction amplitudes

Since the $\Lambda(1405)$ is dynamically generated from the final state interaction of the meson-baryon pair produced, and we also seek for a possible generated resonance from the meson-baryon scattering in $I = 1$, the most general mechanisms for the photoproduction reaction are those depicted in fig. 3. The photoproduction can proceed by the production of either a $\pi\Sigma$ or $\bar{K}N$ pair for $I = 0$ and $I = 1$ and also by $\pi\Lambda$ for the $I = 1$ case. This initial production is represented by the thick circle in fig. 3. The initial meson-baryon pair then rescatters to produce the final $\pi\Sigma$, accounted for by the unitarized scattering amplitude explained in the previous section. Note that a possible contact mechanism of direct $\pi\Sigma$ production would contribute to the background and we do not consider it since a proper background subtraction has been done in the experimental analysis.

Based on fig. 3 it is immediate to realize that the amplitudes for the photoproduction process can be generally written as

$$
\begin{aligned}
t_{\gamma p\to K^+\pi^0\Sigma^0}(W) &= b_0(W)G^{I=0}_{\pi\Sigma}T^{I=0}_{\pi\Sigma,\pi\Sigma}\\
&\quad + c_0(W)G^{I=0}_{\bar{K}N}T^{I=0}_{\bar{K}N,\pi\Sigma}\ ,\\
t_{\gamma p\to K^+\pi^\pm\Sigma^\mp}(W) &= b_0(W)G^{I=0}_{\pi\Sigma}T^{I=0}_{\pi\Sigma,\pi\Sigma}\\
&\quad + c_0(W)G^{I=0}_{\bar{K}N}T^{I=0}_{\bar{K}N,\pi\Sigma}\\
&\quad \pm\sqrt{\frac{3}{2}}\Big(b_1(W)G^{I=1}_{\pi\Sigma}T^{I=1}_{\pi\Sigma,\pi\Sigma}\\
&\quad + c_1(W)G^{I=1}_{\bar{K}N}T^{I=1}_{\bar{K}N,\pi\Sigma}\\
&\quad + d_1(W)G^{I=1}_{\pi\Lambda}T^{I=1}_{\pi\Lambda,\pi\Sigma}\Big)
\end{aligned}
\tag{7}
$$

with W the energy of the γp interaction. The subindex in the b, c and d coefficients stand for the isospin. Note

[1] We neglect the isospin $I = 2$ since it is very small and non-resonant in the energy region of interest in the present work.

that the only difference between the $\gamma p \to K^+\pi^+\Sigma^-$ and the $\gamma p \to K^+\pi^-\Sigma^+$ amplitudes is the sign of the $I = 1$ contributions. The coefficients b, c and d may in general depend on W and hence we consider 9 sets of them in order to account for the 9 different energies W provided by the experimental result of CLAS [2]. On the other hand the relative weight between the different GT addends may be complex in general, therefore we allow the b_1, c_0, c_1 and d_1 to be complex and keep b_0 real since a global phase in the total amplitude is irrelevant. We will refer the b, c and d coefficients by *initial production* (IP) parameters in the following.

Note that, as in ref. [1], we try to keep the analysis as model independent as possible in order to ease its implementation by experimentalist groups. Therefore we intentionally avoid proposing any model for the initial photoproduction mechanisms (filled circle in Fig. 3) which are effectively encoded in the IP parameters. In the actual reaction they would contain a rich dynamics that could count for some contribution from N^* resonances, crossed diagrams, t-channel processes, etc., projected over s-wave. Since we take the coefficients energy dependent, $b(W)$, $c(W)$, $d(W)$ the fit to the data can accommodate this dynamics without explicitly taking it into account.

Since we are fitting 9 different energies, we have in total 81 IP parameters. We are aware that this figure may look large but none of these coefficients affect the meson-baryon scattering amplitude where the resonant dynamics actually stems from. One has to view the fit from the perspective that the data for one energy will provide the small subset of IP parameters for that particular energy. Only the parameters of the potential, that we will consider and explain later in this paper, affect all the data. This situation is similar to the fit conducted to pionic atoms to extract neutron radii in [51]. In that problem there were 19 parameters for 19 neutron radii and 6 parameters for the potential. Again, each of these 19 parameters affected only the data on shifts and widths of a single pionic atom and the 6 parameters of the potential affected all the data. The fits worked without problems and the set of neutron radii obtained is considered nowadays the most valuable experimental source of neutron radii, together with the information obtained from antiprotonic atoms in [52].

We first fit the IP parameters to the photoproduction $\pi\Sigma$ invariant mass distribution data using for the unitarized amplitudes the expression and parameters explained in the previous section. Note that in this first step only the photoproduction vertex is allowed to vary and the chiral unitary approach amplitudes are fixed.

In the evaluation of the theoretical invariant mass distribution the three body phase space has been averaged within the experimental W bin, $[W-0.05, W+0.05]$ GeV, for every W. We perform the fit in the range $M_{\pi\Sigma} \in [1350, 1475]$ MeV. The result of this fit is shown in Fig. 4. One can see that the fit is visually fair for most of the energies, which means that the actual meson-baryon amplitudes must not be much far from those predicted by the chiral unitary approach. However a better χ^2/dof that the one obtained in this fit ($\chi^2/dof = 4.6$) would be desirable.

It is worth stressing again that what we actually want in the present work is not to calculate what the chiral unitary approach predicts for the poles of the $\Lambda(1405)$ or a possible $I = 1$ resonance, but to extract them from the experimental photoproduction data. Therefore we can try to get results with better χ^2/dof by allowing the basic chiral unitary model to vary slightly. In this way we could obtain a fine tuning of the chiral unitary model and then of the position of the $\Lambda(1405)$ poles and try to see if some $I = 1$ resonance shows up. In order to do this we multiply each coefficient of the potentials of the unitary amplitudes, Eqs. (2) and (3), by one real parameter α_i and hence the new coefficient matrices that we consider now are given by

$$C^0_{ij} = \begin{pmatrix} 3\alpha^0_{11} & -\sqrt{\frac{3}{2}}\alpha^0_{12} \\ -\sqrt{\frac{3}{2}}\alpha^0_{12} & 4\alpha^0_{22} \end{pmatrix} \tag{8}$$

for isospin $I = 0$ and

$$C^1_{ij} = \begin{pmatrix} 3\alpha^1_{11} & -\alpha^1_{12} & -\sqrt{\frac{3}{2}}\alpha^1_{13} \\ -\alpha^1_{12} & 2\alpha^1_{22} & 0 \\ -\sqrt{\frac{3}{2}}\alpha^1_{13} & 0 & 0 \end{pmatrix} \tag{9}$$

for isospin $I = 1$.

Furthermore we also allow to vary the subtraction constants from the regularization of the loop functions by multiplying each of them by a free parameter, β_i: $a_{KN} \to \beta_1 a_{KN}$, $a_{\pi\Sigma} \to \beta_2 a_{\pi\Sigma}$ and $a_{\pi\Lambda} \to \beta_3 a_{\pi\Lambda}$. We will refer to the α and β parameters by *potential* parameters in the following (even though the β coefficients do not affect the potential, but we do this just to ease the nomenclature). Therefore, the chiral unitary amplitudes depend on 10 free parameters to be fitted, α_i, β_i, but only 5 of them affect the $I = 0$ amplitude and 7 the $I = 1$. With the potential obtained from the fit we shall search for the positions of the two $\Lambda(1405)$ poles and look for a possible $I = 1$ resonance in the range of energy considered.

If at this point we carry on a global fit allowing for all the parameters to be free from the beginning in the fitting algorithm, there are many local minima of the χ^2 function, most of them having clearly unphysical values of the parameters. Therefore it is very difficult to get and identify an absolute minimum. Actually many minima have χ^2 very similar but with very different values of the parameters, which spoils the statistical significance of the fit and the possible physical conclusions. In order to get physically meaningful results, we implement the following strategy in the line of the one used in ref. [1]: As mentioned above, the previous fit of fig. 4, i.e. fixing the potential parameters to 1, is already reasonably fair, and the potential is consistent with data of scattering [8],

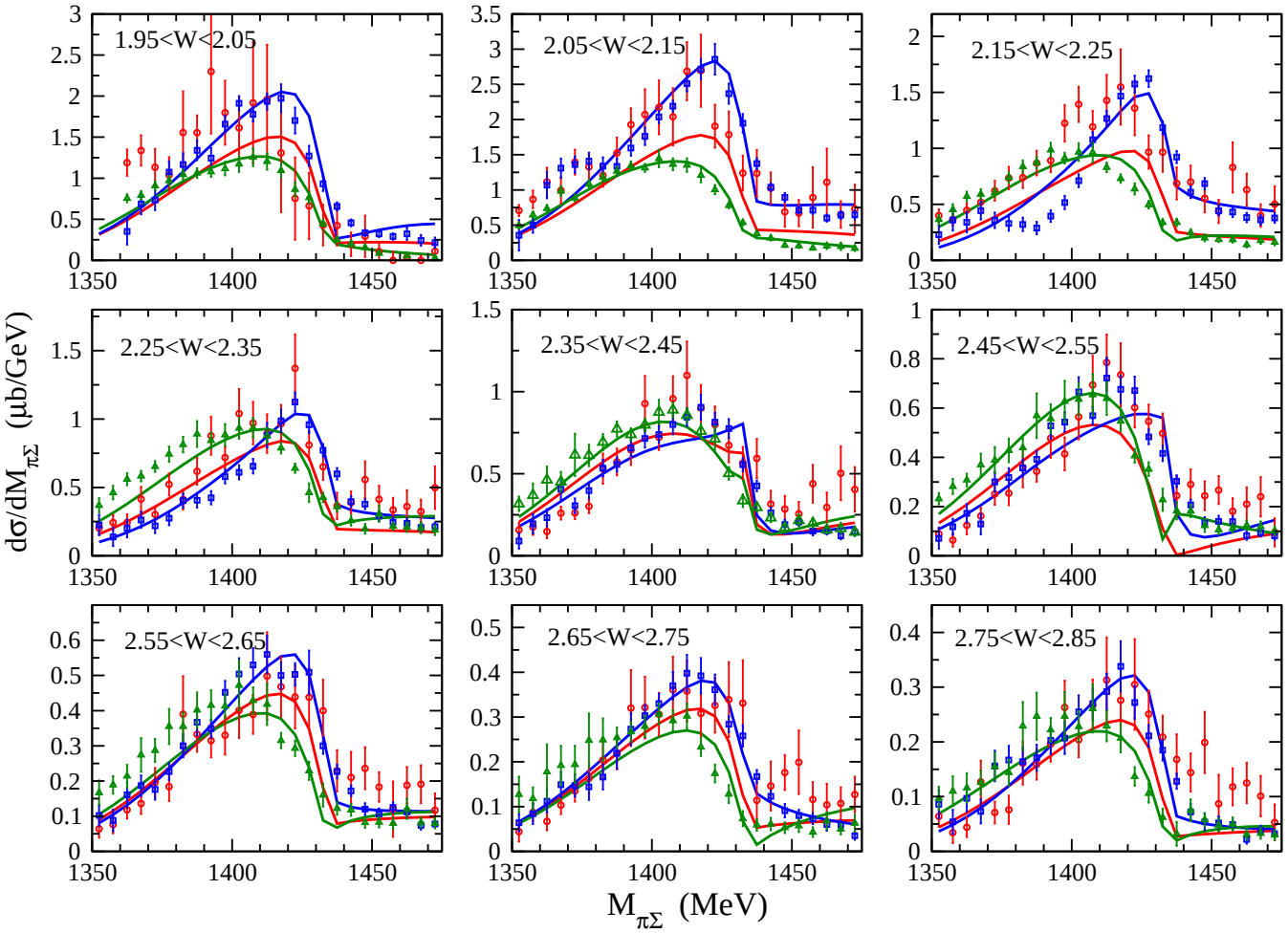

FIG. 4. (Color online) Fit to photoproduction data with fix unitary amplitudes, $\alpha_i = 1$, $\beta_i = 1$. Red: $\pi^0\Sigma^0$; blue: $\pi^-\Sigma^+$, green: $\pi^+\Sigma^-$. Experimental data from ref. [2].

hence a good physical global fit should not be very far from having values of $\alpha_i \sim 1$, $\beta_i \sim 1$. Therefore, in a first step, we start from the fit of fig. 4, which was obtained fixing the potential parameters to 1 ($\alpha_i = 1$, $\beta_i = 1$), but fixing now the IP parameters and allowing only the potential parameters to change. In a next step, we fix the new potential parameters obtained in the previous step and fit again the IP parameters. We iterate the process alternating between fitting the IP or fitting the potential parameters until we get a convergence of the value of the χ^2. In this way we obtain a minimum of the χ^2 with potential parameters not very different from 1 which are then physically meaningful.

After this iterative procedure we get the result shown in fig. 5, which has $\chi^2/dof = 2.1$. The bands account for the uncertainties of the fit at one standard deviation confidence level. The potential parameters obtained are shown in table I.

TABLE I. Parameters of the unitarized amplitudes

α^0_{11}	α^0_{12}	α^0_{22}	α^1_{11}	α^1_{12}	α^1_{13}	α^1_{22}	β_1	β_2	β_3
1.037	1.466	1.668	0.85	0.93	1.056	0.77	1.187	0.722	1.119

It is important to note that the parameters obtained are not very different from one. This means that allowing for just a small variation in the parameters of the chiral unitary approach the photoproduction data can be nicely reproduced.

In table II we show the results obtained for the pole positions in the complex energy ($\sqrt{s}$) plane in unphysical Riemann sheets of the scattering amplitudes. In the table we also show the modulus of the couplings to the different isospin meson-baryon channels obtained from the residues of the unitarized meson-baryon scattering amplitudes at the pole positions, since close to the pole position the amplitude can be approximated by its Laurent expansion where the dominant term is given by

TABLE II. Pole positions (in MeV) in the complex energy plane of the scattering amplitudes and modulus of the couplings to the different channels.

	$I=0$		$I=1$
poles	$1352-48i$	$1419-29i$	–
$\lvert g_{\bar{K}N}\rvert$	2.71	3.06	–
$\lvert g_{\pi\Sigma}\rvert$	2.96	1.96	–

$$T_{ij}(\sqrt{s}) = \frac{g_i\, g_j}{\sqrt{s} - \sqrt{s_{\rm pole}}}, \tag{10}$$

for an s-wave resonance, where the position of the pole can be identified with the mass, M_R, and width, Γ_R, of the resonance by $\sqrt{s_{\rm pole}} = M_R - i\Gamma_R/2$ for a pole not very far from the real axis. Consequently the residue of T_{ij} at the pole position gives $g_i g_j$, where g_i is the effective coupling of the dynamically generated resonance to the i-th channel.

The poles have been looked for in the usual unphysical Riemann sheet of the scattering amplitudes which is defined in the following way: The analytic structure of the scattering amplitude is determined by the loop function G_i (Eq. 5). The G_i function in the second Riemann sheet (RII) can be obtained from the one in the first sheet (RI) by [53]

$$G_i^{II}(\sqrt{s}) = G_i^{I}(\sqrt{s}) + iM_i\frac{q_i}{2\pi\sqrt{s}}, \tag{11}$$

with q_i the center of mass meson or baryon momentum with $\mathrm{Im}(q_i) > 0$. When looking for poles we use $G_j^I(\sqrt{s})$ for $\mathrm{Re}(\sqrt{s}) < m_j + M_j$ and $G_j^{II}(\sqrt{s})$ for $\mathrm{Re}(\sqrt{s}) > m_j + M_j$. This prescription, which we will refer to as usual unphysical Riemann sheet in the following, gives the pole positions closer to those of the corresponding Breit-Wigner forms on the real axis. In this way, no pole is found for $I = 1$ but there is a pole located at $1522 - 14i$ MeV in another unphysical Riemann sheet defined by going to RII for $\pi\Lambda$ and $\pi\Sigma$ channels but not for $\bar{K}N$ despite being above the $\bar{K}N$ threshold (1435 MeV). This pole in this different Riemann sheet does not produce a Breit-Wigner shape in the real axis in the physical sheet but makes the shape of the amplitude below the $\bar{K}N$ threshold to follow the shape of the tail of that pole but then decrease above threshold with a non resonant shape. This means that, for the $I = 1$ amplitudes considered here, even if there is not an explicit pole in the usual unphysical Riemann sheet, an accumulation of strength is present on the real axis in the physical sheet, under the appearance of a cusp. In Figs. 6 and 7 we show the $I = 0$ and $I = 1$ meson-baryon amplitudes with the result of the fit. In Fig. 7, $I = 1$ case, one can see the aforementioned increase of strength and cusp aspect at the $\bar{K}N$ threshold which could be perceived as a resonance in an actual experiment. In order to see that the $I = 1$ amplitude still has to do with a resonant structure, in spite the fact that it does not have a pole in the usual Riemann sheet described above, let us do a mathematical play consisting on varying by hand some of the potential parameter:

Let us change by hand the α^1_{12} parameter, for example, from 0.9 (close to the result of the fit) to 2.3. The resulting $T^{I=1}_{\bar{K}N,\pi\Sigma}$ amplitude and the position of the poles found in different sheets are shown in Figs. 8 and 9. All the poles are found in Riemann sheets for which RI is used for the loop of the $\bar{K}N$ channel. This means that below $\bar{K}N$ threshold (poles represented by circles Fig. 9) the Riemann sheet is the usual unphysical one described above but that is not the case for poles whose real part is located above threshold (poles represented by crosses). We can see that the shape of the resonance gets distorted in a continuous way as we change the parameter.

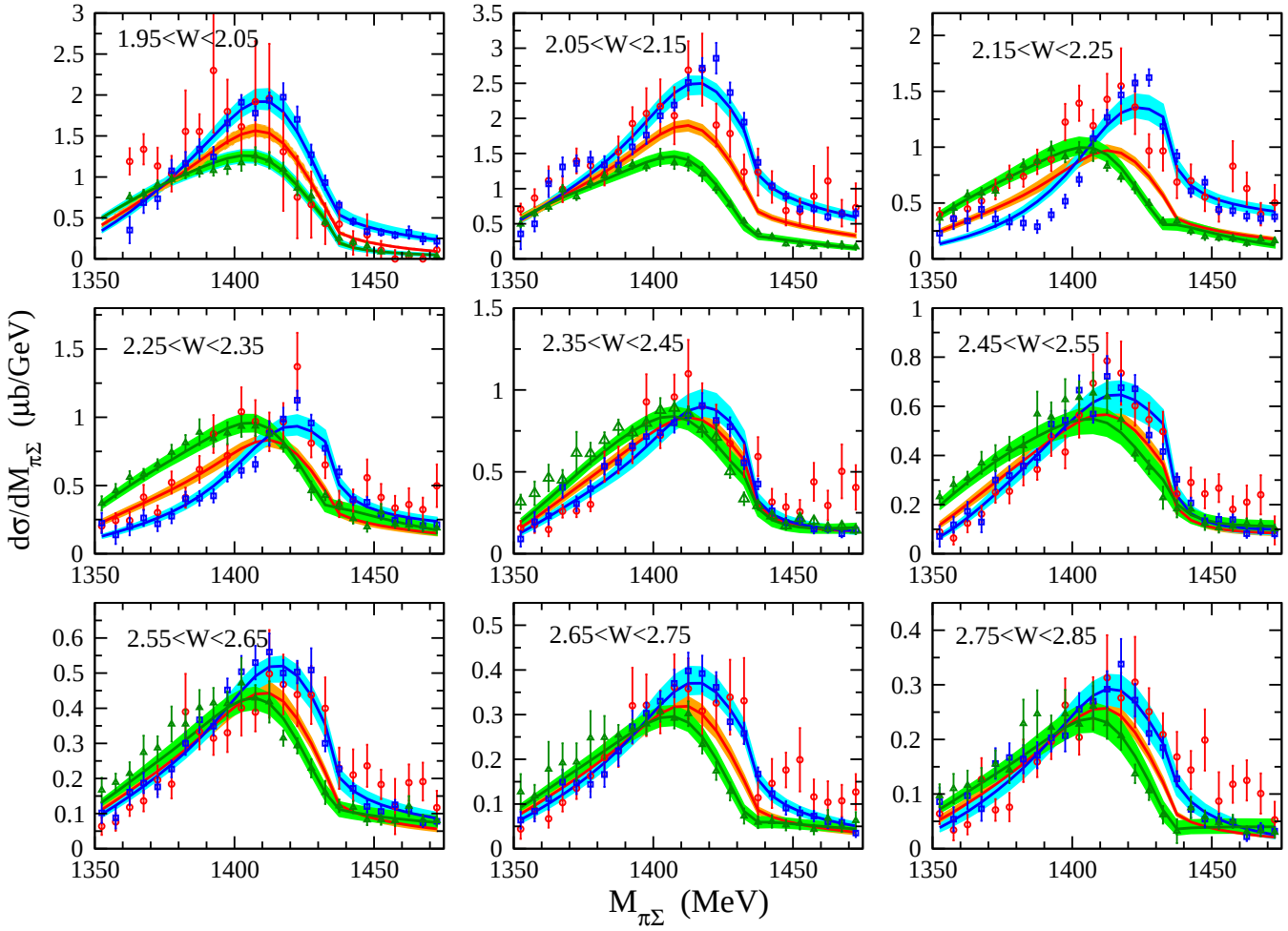

FIG. 5. (Color online) solution from the fit procedure described in the text

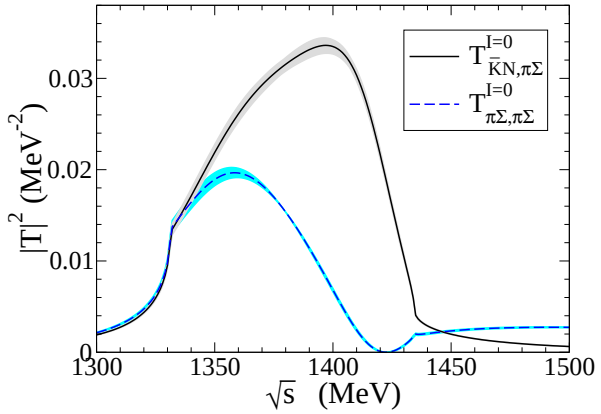

FIG. 6. (Color online) Modulus squared of the $I = 0$ meson-baryon unitarized amplitudes $T^{I=0}_{\pi\Sigma,\pi\Sigma}$ (solid line), $T^{I=1}_{\bar{K}N,\pi\Sigma}$ (dashed line).

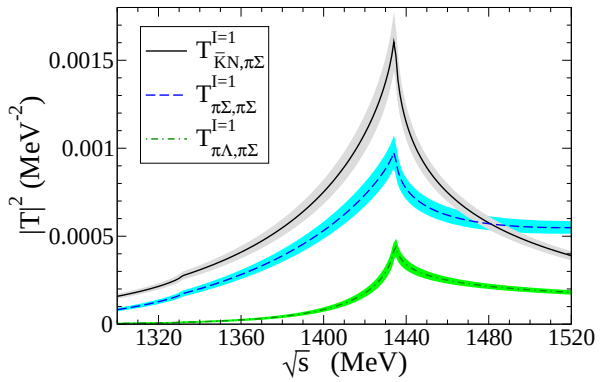

FIG. 7. (Color online) Modulus squared of the $I = 1$ meson-baryon unitarized amplitudes $T^{I=1}_{\pi\Sigma,\pi\Sigma}$ (solid line), $T^{I=1}_{\bar{K}N,\pi\Sigma}$ (dashed line) and $T^{I=1}_{\pi\Lambda,\pi\Sigma}$ (dashed-dotted line) .

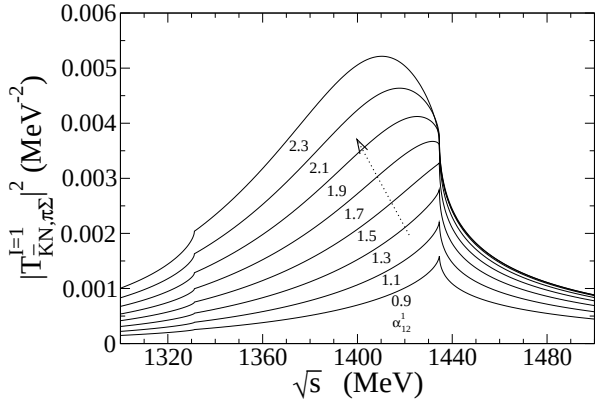

FIG. 8. Evolution of the $I = 1$ $\bar{K}N \to \pi\Sigma$ scattering amplitude ($T^{I=1}_{\bar{K}N,\pi\Sigma}$) as a function of the α^1_{12} coefficient.

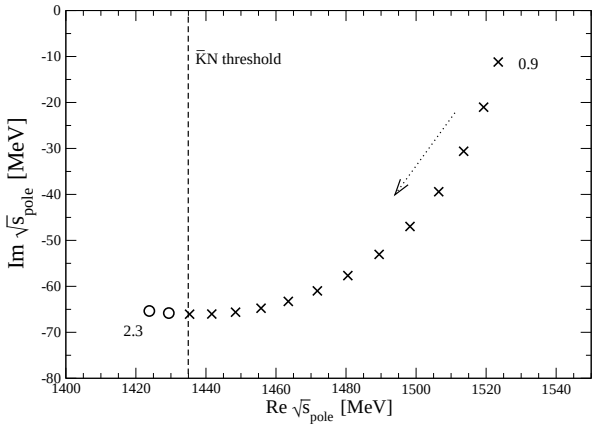

FIG. 9. Evolution of the $I = 1$ pole position as a function of the α^1_{12} coefficient.

However for a short range of the values of the parameter considered, there is a pole in the usual unphysical sheet which eventually disappears from that sheet, when the real part crosses the $\bar{K}N$ threshold. The poles depicted above threshold are in the other unphysical sheet described above. That means that, in spite the fact that there is no pole in the usual unphysical sheet for the particular value of the parameters obtained in the fit, the amplitude is continuously connected with a situation where there is a usual resonance pole and then somehow the amplitude is aware and reflects the existence of the pole for a nearby value of the parameter. This is not a strange case since an analogous situation also shows up for the $a_0(980)$ resonance in the pseudoscalar-pseudoscalar scattering in the scalar isovector channel. In that case there is a pole very close to the $K\bar{K}$ threshold and for small variations in the parameters of the potential the pole disappears from the usual unphysical sheet and goes above threshold to the sheet where the loop function for $K\bar{K}$ is RI. In spite of this fact, everybody considers the $a_0(980)$ as a resonance [46].

In order to make further checks that the fit obtained is physically acceptable, we calculate now the cross section for $K^-p \to MB$ for the meson-baryon final channels K^-p, K^0n, $\pi^+\Sigma^-$, $\pi^-\Sigma^+$, $\pi^0\Sigma^0$ and $\pi^0\Lambda$. The results are shown in Fig. 10 in comparison to experimental data [54]. Note that the results in Fig. 10 are genuine non-trivial predictions since the fit is only done to the photoproduction data. The agreement of the K^-p cross sections to experimental data is remarkable.

Another experimental data usually considered in other theoretical works [55–58] regarding the $\Lambda(1405)$ resonance are the energy shift and width of the kaonic hydrogen in the $1s$ state from the SIDDHARTA experiment at DAFNE [59], which are reported to be $\Delta E - i\Gamma/2 = (283 \pm 42) - i(271 \pm 55)$ eV. This value is related to the K^-p scattering length and therefore to the $K^-p \to K^-p$ amplitude at threshold. (For explicit mathematical expressions see refs. [55–58]). With the values of the parameters in table I we obtain $\Delta E - i\Gamma/2 = (194 \pm 4) -$

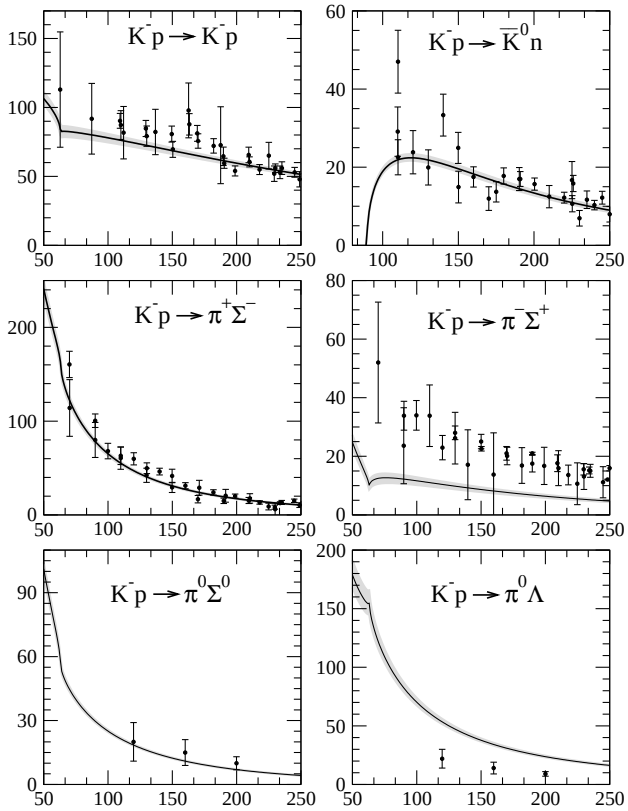

FIG. 10. Predicted $K^- p$ cross sections (in mb). Experimental data from ref. [54].

$i(301 \pm 9)$ eV, which compares reasonably well to the experimental SIDDHARTA data.

On the other hand, in a different fit to the CLAS data made by some members of that collaboration [60], two different kind of fits were performed: one only to the $\pi^0\Sigma^0$ data, to which only the $I = 0$ channel contributes and one to all the photoproduction data. The amplitudes in that fit are parametrized as (Eq.(5) of [60])

$$t_I(m) = C_I(W) e^{i\Delta\phi_I} B_I(m), \tag{12}$$

where $C_I(W)$ is a weight factor, $\Delta\phi_I$ a phase and $B_I(m)$ a Breit-Wigner function. As one can see, the weight is allowed to depend on the photon energy, W, but not its phase. But even more restrictive is the fact that the shapes of the resonances, $B_I(m)$, are Breit-Wigner shapes and chosen independent of the photon energy. This neglects the possibility that the amplitudes $\gamma p \to K^+\pi\Sigma$ are superpositions of the amplitudes corresponding to the different poles with relative weights that depend on the photon energy. Furthermore, as seen in the plots of the amplitudes throughout the present work, the resonant amplitudes are far from being Breit-Wigner like.

With the fit to only the $I = 0$ part introducing two poles, the authors in [60] get for the mass and width of the resonances (all in MeV) $M = 1329$, $\Gamma = 20$, for one of the $I = 0$ resonances and $M = 1390$, $\Gamma = 174$ for the other one. This has to be compared to the fit only to $I = 0$ that we did in ref. [1]; $M = 1368$, $\Gamma = 108$, and $M = 1416$, $\Gamma = 48$ [2]. The differences are due to the reasons explained above and in ref. [1]. The other fit performed in ref. [60] includes two Breit-Wigners for $I = 0$ and one for $I = 1$ and they get $M = 1338$, $\Gamma = 44$, for one of the $I = 0$ resonances and $M = 1384$, $\Gamma = 76$, for the other one and $M = 1357$, $\Gamma = 54$, for the $I = 1$. This fit should be compared to ours in the present paper, (see table II). The difference in the results between our fit and CLAS' is understandable considering the caveats explained above.

IV. SUMMARY

We have implemented an strategy to obtain information on the $I = 0$ and $I = 1$ meson-baryon scattering amplitudes from $\gamma p \to K^+\pi\Sigma$ experimental data. The idea is based on leaving the photoproduction vertices as model independent as possible, to ease the implementation by experimental groups, parametrizing them by coefficients dependent on energy to be fitted to the photoproduction data. The resonant structures come from the meson-baryon final state interaction implemented by amplitudes inspired by the chiral unitary approach but slightly modified with free coefficients. These coefficients and those of the linear combinations were fitted to the data and a good solution is obtained. We provide the position of the two $\Lambda(1405)$ poles (predicted by the chiral unitary approach) and we have discussed the possible existence of an $I = 1$ resonance around the $\bar{K}N$ threshold. In spite the fact that there is not a pole in the usual unphysical Riemann sheet connected to the physical one, we have discussed that there is a resonant structure in $I = 1$ around to the $\bar{K}N$ threshold.

Once the solution of the fit is established, we have obtained fair results for the cross sections of the $K^- p \to MB$ for the meson-baryon final channels $K^- p$, $K^0 n$, $\pi^+\Sigma^-$, $\pi^-\Sigma^+$, $\pi^0\Sigma^0$ and $\pi^0\Lambda$ and for experimental data on kaonic hydrogen.

In the analysis carried out in the present work we show that the information encoded in the photoproduction data is valuable to obtain the information on the resonant content of the $I = 0$ and $I = 1$ channels in the energy region considered.

Concerning the I=1 amplitude, we showed that the situation is very similar to the one of the $a_0(980)$ resonance, which is accepted as a resonance. Whether one decides to call or not a resonance the $I = 1$ pole that we find in an unusual Riemann sheet, the resonant like structure

[2] Note that there is a slight difference between these values and those reported in ref. [1]. This is due to a change in some of the CLAS experimental data from those reported in [34] to those in [2].

in the real axis has important repercussion in the photoproduction amplitudes and we can expect it to have important effects in many other observables. Since the relevant information is the I=1 amplitude in the real axis, the present work has provided values for this amplitude which can be tested in the study of future reactions.

ACKNOWLEDGMENTS

This work is partly supported by the Spanish Ministerio de Economia y Competitividad and European FEDER funds under the contract number FIS2011-28853-C02-01, and the Generalitat Valenciana in the program Prometeo, 2009/090. We acknowledge the support of the European Community-Research Infrastructure Integrating Activity Study of Strongly Interacting Matter (acronym HadronPhysics3, Grant Agreement n. 283286) under the Seventh Framework Programme of EU.

[1] L. Roca and E. Oset, Phys. Rev. C **87**, 055201 (2013)
[2] K. Moriya *et al.* [CLAS Collaboration], Phys. Rev. C **87**, 035206 (2013).
[3] R. H. Dalitz, S. F. Tuan, Annals Phys. **10**, 307-351 (1960).
[4] R. H. Dalitz, T. C. Wong, G. Rajasekaran, Phys. Rev. **153**, 1617-1623 (1967).
[5] E. A. Veit, B. K. Jennings, R. C. Barrett, A. W. Thomas, Phys. Lett. **B137**, 415 (1984).
[6] N. Kaiser, P. B. Siegel and W. Weise, Nucl. Phys. A **594**, 325 (1995).
[7] N. Kaiser, T. Waas and W. Weise, Nucl. Phys. A **612**, 297 (1997).
[8] E. Oset and A. Ramos, Nucl. Phys. A **635**, 99 (1998).
[9] J. A. Oller and U. G. Meissner, Phys. Lett. B **500**, 263 (2001).
[10] M. F. M. Lutz and E. E. Kolomeitsev, Nucl. Phys. A **700**, 193 (2002).
[11] E. Oset, A. Ramos and C. Bennhold, Phys. Lett. B **527**, 99 (2002) [Erratum-ibid. B **530**, 260 (2002)].
[12] T. Hyodo, S. I. Nam, D. Jido and A. Hosaka, Phys. Rev. C **68**, 018201 (2003).
[13] D. Jido, J. A. Oller, E. Oset, A. Ramos, U. G. Meissner, Nucl. Phys. **A725**, 181-200 (2003).
[14] C. Garcia-Recio, J. Nieves, E. Ruiz Arriola and M. J. Vicente Vacas, Phys. Rev. D **67**, 076009 (2003).
[15] C. Garcia-Recio, J. Nieves and L. L. Salcedo, Phys. Rev. D **74**, 034025 (2006).
[16] B. Borasoy, R. Nissler and W. Weise, Eur. Phys. J. A **25**, 79 (2005).
[17] J. A. Oller, Eur. Phys. J. A **28**, 63 (2006).
[18] B. Borasoy, U. G. Meissner and R. Nissler, Phys. Rev. C **74**, 055201 (2006).
[19] Y. Ikeda, T. Hyodo and W. Weise, Nucl. Phys. A **881**, 98 (2012).
[20] K. P. Khemchandani, A. Martinez Torres, H. Kaneko, H. Nagahiro and A. Hosaka, Phys. Rev. D **84**, 094018 (2011).
[21] T. Hyodo and D. Jido, Prog. Part. Nucl. Phys. **67**, 55 (2012).
[22] Z. -H. Guo and J. A. Oller, Phys. Rev. C **87**, 035202 (2013).
[23] P. J. Fink, Jr., G. He, R. H. Landau and J. W. Schnick, Phys. Rev. C **41**, 2720 (1990).
[24] J. Beringer *et al.* [Particle Data Group Collaboration], Phys. Rev. D **86**, 010001 (2012).
[25] J. C. Nacher, E. Oset, H. Toki and A. Ramos, Phys. Lett. B **461**, 299 (1999).
[26] T. Hyodo, A. Hosaka, E. Oset, A. Ramos and M. J. Vicente Vacas, Phys. Rev. C **68**, 065203 (2003).
[27] V. K. Magas, E. Oset and A. Ramos, Phys. Rev. Lett. **95**, 052301 (2005).
[28] L. S. Geng and E. Oset, Eur. Phys. J. A **34**, 405 (2007).
[29] B. Borasoy, P. C. Bruns, U. -G. Meissner and R. Nissler, Eur. Phys. J. A **34**, 161 (2007).
[30] D. W. Thomas, A. Engler, H. E. Fisk and R. W. Kraemer, Nucl. Phys. B **56**, 15 (1973).
[31] R. J. Hemingway, Nucl. Phys. B **253**, 742 (1985).
[32] M. Niiyama, H. Fujimura, D. S. Ahn, J. K. Ahn, S. Ajimura, H. C. Bhang, T. H. Chang and W. C. Chang *et al.*, Phys. Rev. C **78**, 035202 (2008).
[33] S. Prakhov *et al.* [Crystall Ball Collaboration], Phys. Rev. C **70**, 034605 (2004).
[34] K. Moriya *et al.* [CLAS Collaboration], AIP Conf. Proc. **1441**, 296 (2012).
[35] K. Moriya *et al.* [CLAS Collaboration], arXiv:1305.6776 [nucl-ex].
[36] I. Zychor, M. Buscher, M. Hartmann, A. Kacharava, I. Keshelashvili, A. Khoukaz, V. Kleber and V. Koptev *et al.*, Phys. Lett. B **660**, 167 (2008).
[37] G. Agakishiev, A. Balanda, D. Belver, A. V. Belyaev, J. C. Berger-Chen, A. Blanco, M. Bohmer and J. L. Boyard *et al.*, arXiv:1208.0205 [nucl-ex].
[38] J. Siebenson and L. Fabbietti, arXiv:1306.5183 [nucl-ex].
[39] O. Braun, H. J. Grimm, V. Hepp, H. Strobele, C. Thol, T. J. Thouw, D. Capps and F. Gandini *et al.*, Nucl. Phys. B **129**, 1 (1977).
[40] H. Y. Lu *et al.* [CLAS Collaboration], arXiv:1307.4411 [nucl-ex].
[41] J. -J. Wu, S. Dulat and B. S. Zou, Phys. Rev. C **81** (2010) 045210.
[42] P. Gao, J. -J. Wu and B. S. Zou, Phys. Rev. C **81**, 055203 (2010).
[43] T. Hyodo, D. Jido, and A. Hosaka, Phys. Rev. **D75**, 034002 (2007).
[44] V. Bernard, N. Kaiser and U. G. Meissner, Int. J. Mod. Phys. E **4** (1995) 193.
[45] A. Dobado and J. R. Peláez, Phys. Rev. D **56** (1997) 3057.
[46] J. A. Oller, E. Oset and J. R. Pelaez, Phys. Rev. D **59** (1999) 074001 [Erratum-ibid. D **60** (1999) 099906].
[47] J. A. Oller and E. Oset, Phys. Rev. D **60** (1999) 074023.

[48] T. Hyodo, S. I. Nam, D. Jido, and A. Hosaka, Prog. Theor. Phys. **112**, 73 (2004).
[49] J. A. Oller and E. Oset, Nucl. Phys. A **620** (1997) 438 [Erratum-ibid. A **652** (1999) 407].
[50] T. Hyodo and D. Jido, Prog. Part. Nucl. Phys. **67** (2012) 55.
[51] C. Garcia-Recio, J. Nieves and E. Oset, Nucl. Phys. A **547**, 473 (1992).
[52] A. Trzcinska, J. Jastrzebski, P. Lubinski, F. J. Hartmann, R. Schmidt, T. von Egidy and B. Klos, Phys. Rev. Lett. **87**, 082501 (2001).
[53] L. Roca, E. Oset and J. Singh, Phys. Rev. D **72** (2005) 014002.
[54] G. S. Abrams, B. Sechi-Zorn, Phys. Rev. **139** (1965) B454; M. Sakitt, et al., Phys. Rev. **139** (1965) B719; J. K. Kim, Phys. Rev. Lett. **14** (1965) 29; M. Csejthey-Barth, et al., Phys. Lett. **16** (1965) 89; T. S. Mast, et al., Phys. Rev. **D14** (1976) 13; R. O. Bangerter, et al., Phys. Rev. **D23** (1981) 1484; J. Ciborowski, et al., J. Phys. **G8** (1982) 13; D. Evans, et al., J. Phys. **G9** (1983) 885.
[55] Z. -H. Guo and J. A. Oller, Phys. Rev. C **87** (2013) 035202.
[56] M. Mai and U. -G. Meissner, Nucl. Phys. A **900** (2013) 51.
[57] Y. Ikeda, T. Hyodo and W. Weise, Phys. Lett. B **706**, 63 (2011).
[58] Y. Ikeda, T. Hyodo and W. Weise, Nucl. Phys. A **881**, 98 (2012).
[59] M. Bazzi, G. Beer, L. Bombelli, A. M. Bragadireanu, M. Cargnelli, G. Corradi, C. Curceanu (Petrascu) and A. d'Uffizi *et al.*, Phys. Lett. B **704**, 113 (2011).
[60] R. A. Schumacher and K. Moriya, arXiv:1303.0860 [nucl-ex].